Posttranslational Heterocyclization of Cysteine and Serine Residues in the Antibiotic Microcin B17: Distributivity and Directionality†

Neil L. Kelleher,‡ Christopher L. Hendrickson,§ and Christopher T. Walsh*,‡

Department of Biological Chemistry and Molecular Pharmacology, Harvard Medical School, Boston, Massachusetts 02115, and National High Magnetic Field Laboratory, Florida State University, Tallahassee, Florida 32310

Received June 15, 1999

ABSTRACT: To produce the antibiotic Microcin B17, four Cys and four Ser residues are converted into four thiazoles and four oxazoles by the three subunit Microcin B17 synthetase. High-resolution mass spectrometry (MS) was used to monitor the kinetics of posttranslational heterocyclic ring formation (−20 Da per ring) and demonstrated the accumulation of all intermediates, from one to seven rings, indicating distributive processing. All of the intermediates could be converted by the enzyme to the eight ring product. Enzymatic chemoselectivity (Cys vs Ser cyclization rates) was assessed using iodoacetamido-salicylate to alkylate unreacted cysteines (+193 Da) in the 8 kDa biosynthetic intermediates; three of the first four rings formed were thiazoles, and by the five ring stage, all four of the cysteines had been heterocyclized while three of the original four serines remained uncyclized. Finally, tandem MS using a 9.4 T Fourier transform instrument with electrospray ionization was used to elaborate the major processing pathway: the first two rings formed are at the most amino proximal sites (Cys^{41} then Ser^{40}) followed by the remaining three cysteines at positions 48, 51, and 55. The cyclization of serines at positions 56, 62, and 65 then follows, with Ser^{62} and Ser^{65} the last to heterocyclize and the first of these at a slower rate. Thus, despite free dissociation of intermediates after each of seven ring-forming catalytic cycles, there is an overall directionality of ring formation from N-terminal to C-terminal sites. This remarkable regioselectivity is determined more by the substrate than the enzyme, due to a combination of (1) initial high-affinity binding of the posttranslational catalyst to the N-terminal propeptide of substrate 88mer, and (2) a chemoselectivity for thiazole over oxazole formation. This mechanism is consistent with antibiotic biosynthesis in vivo, yielding microcin with six, seven, and eight rings, all with bioactivity.

The microcins are a structurally diverse group of molecules below ~10 kDa excreted from various bacteria (*1*). Structural characterization of several of these antibiotics has now been completed, including the biosynthetic genes and the nature of posttranslational modifications. During maturation of the polypeptide antibiotic Microcin B17 from certain strains of *Escherichia coli*, the 3 component McbB, -C, and -D synthetase generates tandem 4,2-bisheterocycles from the tripeptide sequences $Gly^{39}Ser^{40}Cys^{41}$ and $Gly^{54}Cys^{55}Ser^{56}$ in the 69 amino acid substrate McbA, as well as 2 monocyclic thiazoles and 2 oxazoles at other Gly-Cys and Gly-Ser sites. Of the eight rings formed, four are thiazoles in the middle region of the substrate (Scheme 1). To determine chemoselectivity and regioselectivity preferences of Microcin B17 synthetase for its substrate and to gain insight into the mechanism of this type of natural product biosynthesis, we report on a tandem mass spectrometric approach to locate the heterocycles in full-length McbA intermediates and product. We present here mechanistic insights into the ring formation process by quantitation and microcharacterization of MccB17 biosynthetic intermediates by high-resolution tandem mass spectrometry (MS).

Microcin B17 (MccB17)[1] is thought to cause double-stranded DNA cleavage in a DNA gyrase dependent mechanism (*2*). With use of the cofactors ATP, reduced FMN, and Zn^{2+} by McbD, McbC, and McbB, respectively, the holo-synthetase causes cyclization of four Cys and four Ser residues on the upstream amide carbonyl. The overall maturation pathway of MccB17 was elucidated by Kolter and co-workers (*3, 4*) and is outlined in Scheme 1. For each ring formed, a loss of 20.03 Da in mass results due to loss of H_2O (dehydration, −18.01 Da) and H_2 (oxidation, −2.02 Da). McbD contains an N-terminal ATP binding site, although ATP is not involved directly in heterocycle formation (ATP hydrolysis can be uncoupled from heterocyclization) (*5*). The leader peptide (residues 1−26 in McbA) is

† This research was supported by the National Institutes of Health (C.T.W., GM 20011; N.L.K., postdoctoral fellowship F32 AI 10087-02) and the National Science Foundation (National High-Field FT-ICR MS Facility, NHMFL, NSF CHE-94-13008). N.L.K. also received support from the Harvard Armenise Foundation.

* Corresponding author. Phone: (617) 432-1715. Fax: (617) 432-0556. E-mail: walsh@walsh.med.harvard.edu.

‡ Harvard Medical School.

§ Florida State University.

[1] Abbreviations: ATP, adenosine triphosphate; CAD, collisionally activated dissociation; CBP, calmodulin binding peptide; DTT, dithiothreitol; EDTA, ethylenediaminetetraacetic acid; ESI, electrospray ionization; FMN, flavin mononucleotide; FTMS, Fourier transform mass spectrometry; IRMPD, infrared multiphoton dissociation; IPTG, isopropyl 1-thio-β-D-galactopyranoside; MccB17, Microcin B17; MS, mass spectrometry; MS/MS, tandem MS; SORI, sustained off-resonance irradiation; SWIFT, stored-waveform inverse Fourier transform; T, tesla; TCEP, tris(carboxyethyl)phosphine hydrochloride.

10.1021/bi9913698 CCC: $18.00
Published on Web 11/03/1999

Scheme 1: Sequence of McbA (69 Residues) and Its Maturation Pathway to Mature Microcin B17

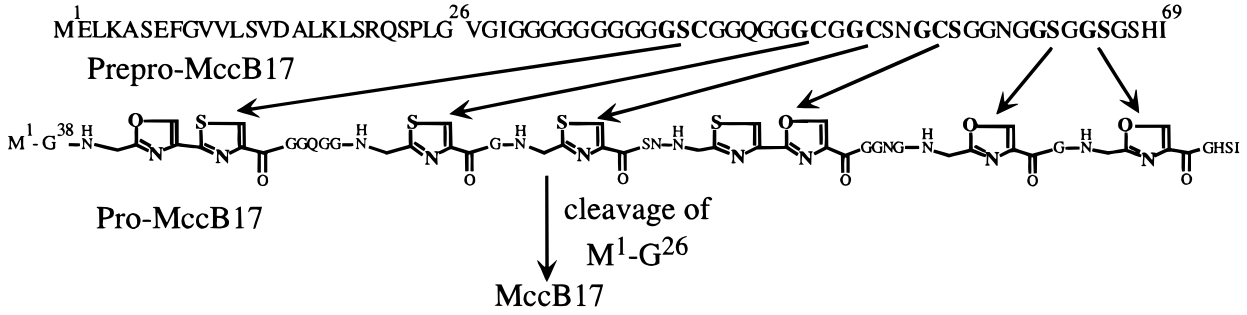

essential (*6*) and has been shown to be the primary recognition element for the synthetase (*7*).

We have shown previously that for truncated two site substrate versions of McbA (McbA$_{1-46}$), the enzyme releases the one ring intermediate (*8*), and we have characterized the regioselectivity for the first bis-heterocyclization site (*9*), a tandem 4,2-oxazole−thiazole. Further, the reverse regioisomer, Gly^{39}Cys^{40}Ser^{41}, in the McbA$_{1-46}$ fragment stopped at an M-20 monocyclic product. The Cys^{40} and Cys^{41} mutant regioisomers of McbA$_{1-46}$ (*9*), Gly^{39}Cys^{40}Gly^{41} and Gly^{39}-Gly^{40}Cys^{41}, served as enzymatic substrates and yielded M-20 products with thiazoles at specified locations to serve as standards for tandem MS (MS/MS) fragmentation. This established that heterocycle formation blocks chain fragmentation on both sides of the ring, fingerprinting the location of the heterocycle in the sequence (*9*). The regioselectivity of processing of wild-type McbA$_{1-46}$ (GSC) and three mutants, GCS, GCC, and GSS, to M-20 intermediates could then be analyzed.

Fourier transform (FT) mass spectrometry (*10*) coupled with electrospray ionization (ESI) (*11*) was initially described in 1989 and has unique capabilities for >5 kDa ions, including resolution of isotopic peaks for proteins *and* their fragmentation products produced during MS/MS (*12*). Here, these ESI/FTMS advantages have allowed kinetic and structural characterization of biosynthetic intermediates of varying ring content in full-length McbA (1−69) and permitted deconvolution of chemoselectivity, directionality, and distributivity in the remarkable series of enzyme-catalyzed maturation steps for prepro-Microcin B17.

EXPERIMENTAL PROCEDURES

Strains and Plasmids. Plasmids pET15b(+)His$_6$-McbA encoding a hexahistidine affinity tag fused to the McbA structural gene (*13*) and pCalBCDn encoding the three subunits of microcin synthetase have been described earlier (*14*). Expression of His$_6$-McbA and microcin synthetase was carried out in *E. coli* BL21(DE3). The sequence encoded by the His$_6$-McbA construct (88 amino acids; Figure 7a) is numbered to preserve previous Microcin B17 numbering schemes.

Site-Directed Mutagenesis. The Ser^{65}→Cys^{65} mutant of His$_6$-McbA was generated by SOE-PCR (*15*) using the following primers: 5′-CTCATGTTTGACAGCTTATCATCG-3′ (outside primer, coding strand) and 5′-CCGCAAGGAA-TGGTGCATGCAAGG-3′ (outside primer, noncoding strand); mutagenic primers 5-TCAGATATGTGAACCACATCCGC-CGCTGCCACCGTTTCC-3′ (coding strand) and 5′-AACG-GTGGCAGCGGCGGATGTGGTTCACATATCTGAGG-3′ (noncoding strand).

Microcin B17 Synthetase and Substrates. Samples of synthetase were prepared using calmodulin binding protein (CBP) fusion to McbB and affinity purified as described elsewhere (*14*). Cells harboring pET15b(+)His$_6$-McbA were grown in 3 × 1 L of LB medium to an OD$_{595}$ of ∼0.7 and induced with 1 mM IPTG. After 3−4 h, the cells were harvested and lysed by french press (lysis buffer = 20 mM Tris-HCl, pH 7.9, 500 mM NaCl, 5 mM imidazole). The extract was spun for 35 min at 35 000 rpm and the supernatant applied to a Ni^{2+} affinity column (Novagen) with a 2.5 mL bed volume. The column was washed with 10 column volumes of lysis buffer and eluted with stripping buffer (20 mM Tris, pH 7.9, 500 mM NaCl, 100 mM EDTA). One milliliter fractions were collected, and those containing His$_6$-McbA visible on a Coomassie-stained SDS gel (15%) were pooled and dialyzed overnight against 50 mM Tris, 1 mM EDTA, 5 mM DTT, pH 7.5.

Kinetics of Ring Formation. His$_6$-McbA substrate (10−200 μL of 0.7 mg/mL) was mixed with 100−200 μL of synthetase and 10 × assay buffer (500 mM Tris, pH 7.5, 1 M NaCl, 200 mM $MgCl_2$, 100 mM DTT, 20 mM ATP). Samples were quenched at various time points by the addition of 6 M urea to a final concentration of 1 M, and injected onto a C18 reversed-phase HPLC column. Heterocyclic ring formation was monitored at A_{254} and A_{280} and did not change the retention time significantly (*8*); substrates eluted at 9 min in a 12 min linear gradient of 25−40% acetonitrile. Typical samples gave an A_{220} of 0.1−1. The ∼1.25 mL of eluent was lyophilized and the sample redissolved in 60:38:2 MeOH/H_2O/HOAc for ESI. For some samples, further desalting using a reversed-phase peptide trap (0.1 mm i.d.; Michrom BioResources, Auburn, CA) was required to minimize sodium and potassium adducts (<5% relative abundance).

Proteolytic Cleavage of Leader Peptide. Dried samples of processed His$_6$-McbA were resuspended in 100 μL of 50 mM Tris, pH 8.3, 1 mM EDTA; 3 μL of α-chymotrypsin (12 μM stock in 50 mM Tris, 1 mM EDTA, pH 7.5) was added to the reaction which was quenched after 1−2 h by freezing (−80 °C) or injection onto a C18 reversed-phase column. Using a linear gradient of 10−30% CH_3CN over 40 min, the biosynthetic intermediates resulting from chymotryptic cleavage of the Leu^{25}−Gly^{26} bond eluted from 15 to 20 min, with increasing ring content resulting in longer retention times.

Alkylation of Biosynthetic Intermediates. HPLC-purified, processed His$_6$-McbA was treated with 5 mM 4-(iodoacet-

amido)salicylic acid in 50 mM Tris, pH 8.5, 1 mM EDTA, 2 M guanidine hydrochloride, 5 mM TCEP, for 2 h at room temperature. HPLC was required to desalt the samples and separate excess alkylation reagent from the alkylated forms of substrate; one broad peak from 9 to 10.5 min was collected, lyophilized, and redissolved in 50 μL of 80:18:2 MeOH/H_2O/HOAc.

Electrospray Ionization. Desalted solutions containing 20−70 μM His_6-McbA (1−5 μL) were loaded into a Nanospray tip (*16*) (New Objective, Inc., Cambridge, MA) with a 2 or 4 μm i.d. tip; an ESI voltage of 0.6−1.5 kV applied to the solution by a platinum wire produced ∼10−50 nL/min flow rates. For extended spraying times, 20−200 μL of sample was infused at 300 nL/min into a fused silica capillary terminated with a fused silica ESI tip (25 μm i.d. tip) ground to a conical shape. The ESI voltage (1.2−2.5 kV) was applied to the metal union between the transfer capillary (50 μm i.d. by 360 μm o.d.) and the tip.

Mass Spectrometry. Three different FTMS systems were used in this study. The construction and operation of the 4.7 T (*17*), the 6.1 T (*18*), and the 9.4 T (*19*) systems are as described in the references cited. In general, ions from electrospray are directed through a metal capillary, skimmer, and multiple ion guides into the ion cell (10^{-9}−10^{-10} torr) of the FTMS. The operation of the 9.4 and 4.7 T systems differed from the 6.1 T system in that ions are accumulated in the ion guides external to the magnet bore rather than in the ion cell, respectively (see Results). Fragmentation of ions entering the FTMS employed nozzle−skimmer (NS) dissociation (*20*) with a 200 V potential difference on the 6.1 T instrument. Theoretical isotopic distributions were generated using Isopro v3.0 (*21*) and fit to experimental data by least squares to assign the most abundant isotopic peak. The mass difference (in units of 1.0034 Da) between the most abundant isotopic peak and the monoisotopic peak is denoted in italics after each molecular mass value. Spectra were calibrated externally using bovine ubiquitin, 8564.64-*5* Da. Transients were stored with an Odyssey (Finnigan FT/MS) or an XMASS Data Station (Bruker Daltonics) as 128, 256, or 512 K data sets.

Tandem MS (MS/MS). MS/MS of His_6-McbA biosynthetic intermediates was performed using the 9.4 T instrument. Desired ions were isolated using chirp excitations to remove all charge states from 500 to 2000 *m/z* of the analyte except the one targeted for MS/MS, followed by a stored waveform inverse Fourier transform (SWIFT) (*22*) pulse with a narrow bandwidth to isolate the ions of a given biosynthetic intermediate. Collisionally activated dissociation (CAD) was accomplished using sustained off-resonance irradiation (SORI) (*23*) for 1.25 s at 1.2−1.6 kHz off-resonance from the precursor ion and ∼10^{-6} torr Ar or N_2. For infrared multiphoton dissociation (IRMPD), a 40 W infrared laser (*24*) was used for 60−300 ms at 50% power.

RESULTS

His_6-McbA Substrate Ions. A broadband ESI/FT mass spectrum of the His_6-McbA gene product showed multiply protonated ions, with charge states ranging from 10+ to 6+ (Figure 1). A relative molecular mass (M_r) value of 8039.67-*4* Da was measured for the 9+ ions (Figure 1, inset). This value corresponds to the DNA-predicted value of 8043.68-*4* Da if the four predicted Cys residues are involved in two intramolecular disulfide bonds (−4.03 Da). Reaction of this His_6-McbA sample with DTT increased the observed M_r value by 4.01 Da (not shown), indicating a correct primary sequence.

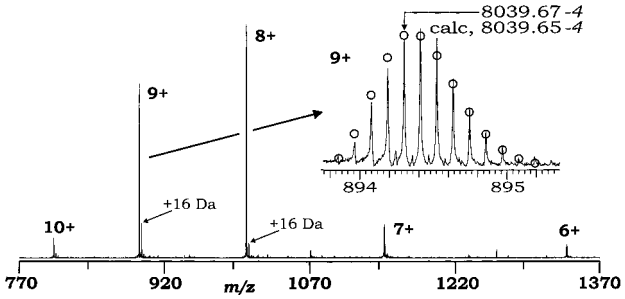

FIGURE 1: Broadband ESI/FT mass spectrum of His_6-McbA ions. The inset shows expansion of the $(M+9H^+)^{9+}$ ions; open circles, theoretical isotopic distribution for the gene product with 2 disulfide bonds; single scan, 6.1 T data.

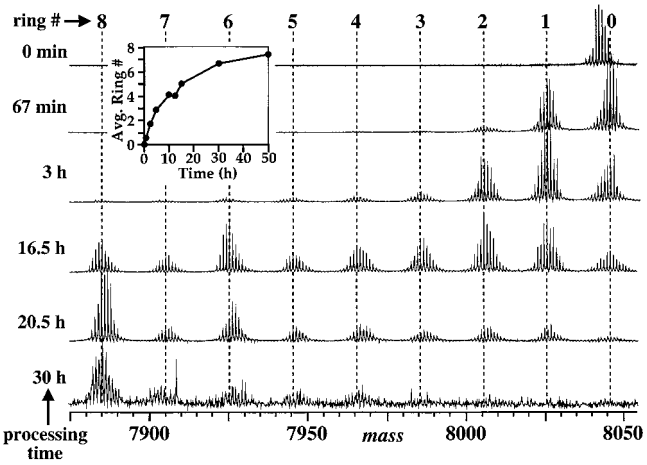

FIGURE 2: Action of CBP-tagged microcin synthetase on the His_6-McbA substrate vs time. 9+ ions, all single scan, 6.1 T data; inset: plot of average heterocycle content of each sample vs time (spectrum at 50 h not shown).

Enzymatic Processing of His_6-McbA Substrate. Analysis of His_6-McbA incubated with affinity-purified microcin synthetase for 67 min, 3 h, 16.5 h, 20.5 h, and 30 h revealed a large relative abundance of every biosynthetic intermediate containing one to seven rings (Figure 2). The mass difference between each intermediate is 20.02 ± 0.04 (Figure 2, dashed vertical lines), consistent with cyclization, dehydration ($-H_2O = -18.01$ Da), and aromatization ($-H_2 = -2.02$ Da) occurring in a closely coupled fashion (i.e., no M−2 or M−18 Da species are observed). For cyclization by the CBP-tagged synthetase, the initial ring formation rate is 0.5 h^{-1}, and the apparent half-life for the synthetase activity under these incubation conditions is 4 h (inset, Figure 2). For a preparation of wild-type synthetase (*13*), time points taken at 3, 5, and 15 h yielded data analogous to those of Figure 2. Additionally, purification of MccB17 from an *E. coli* producing strain [ZK15, (*25*)] showed in vivo intermediates containing six and seven rings, in addition to the mature antibiotic with eight rings (Figure 3), consistent with dissociation events between ring-forming catalytic cycles. The buildup of biosynthetic intermediates with one to seven rings with purified synthetase in vitro permits interrogation of kinetic and chemical preferences of the enzyme during maturation of McbA.

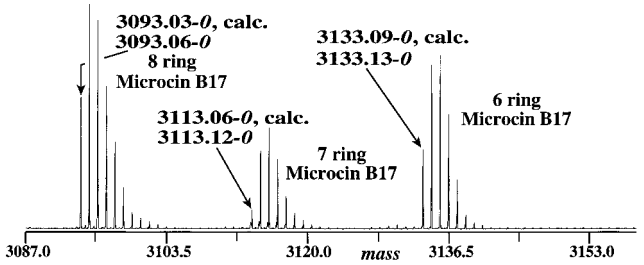

FIGURE 3: Microcin B17 purified from an *E. coli* strain harboring the plasmid-encoded MccB17 biosynthetic and immunity operon.

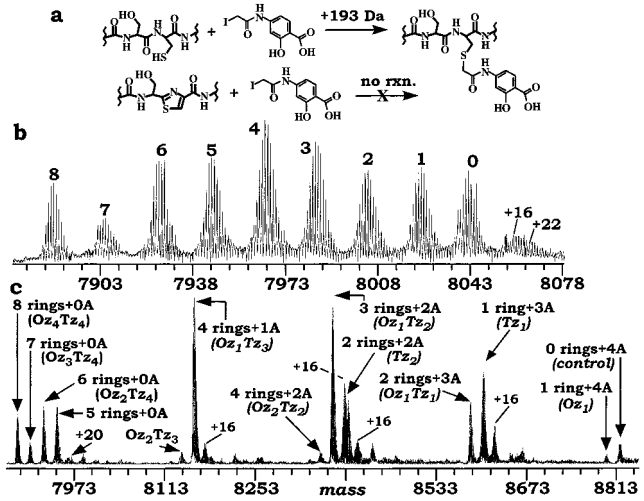

FIGURE 4: (a) Differential reactivity of 4-(iodoacetamido)salicylic acid toward Cys vs thiazole rings and Ser. (b) Spectrum of $(His_6\text{-McbA})^{7+}$ ions after 7.5 h of synthetase processing; numbers indicate ring content; 9.4 T, single scan data. (c) Spectrum of the same mixture from (b) after alkylation with 4-(iodoacetamido)salicylic acid; A, +193 Da; Oz, oxazole; Tz, thiazole; +16, oxygen atom addition due to oxidation; subscripts denote number of rings, not their position in substrate 88mer; 9.4 T, single scan data.

Composition of Biosynthetic Intermediates: Counting Thiazole (Tz) and Oxazole (Oz) Rings. Treatment of the substrate preparations of His_6-McbA with 4-(iodoacetamido)-salicylic acid resulted in a 772.21 Da increase in the M_r value, expected for alkylation of all four cysteine residues ($4 \times 193.04 = 772.15$ Da, data not shown). Since thiazole rings are not alkylated (*9*), we could analyze whether various intermediates contained uncyclized cysteines by looking for mass shifts in increments of 193 mass units (Figure 4a). Treatment of His_6-McbA with CBP-tagged synthetase for 7.5 h gave the Figure 4b data, again showing the distributive display of intermediates. Treatment of this mixture with 4-(iodoacetamido)salicylic acid yielded the spectrum shown in Figure 4c. The species with eight, seven, and six rings formed show no increase in their M_r values, indicating that all four Cys residues have been converted to thiazoles by the six ring stage. The five ring material shows a ~4:1 split between zero and one alkylation events (A = alkylation event in Figure 4c), respectively, indicating mainly an Oz_1Tz_4 composition (minor Oz_2Tz_3). The intermediate(s) with four

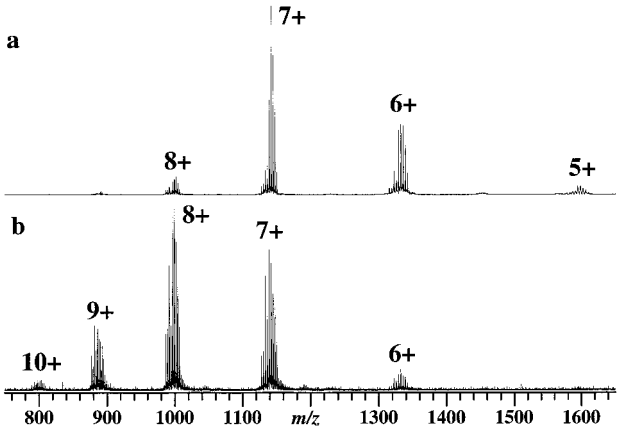

FIGURE 5: Broadband ESI/FT mass spectra (9.4 T) of His_6-McbA acquired in the external (a) or internal (b) ion accumulation mode after 5 and 12 h of microcin synthetase processing, respectively.

rings show a 193.01 Da increase in M_r value, undergoing one alkylation event (+193.04 Da, theory). This reveals that three of the four thiazoles have formed in the four ring species, leaving only one free cysteine thiol available for alkylation, and that one of the four rings must be an oxazole (i.e., an Oz_1Tz_3 species). The three ring intermediate has added 386.11 Da, undergoing two alkylation reactions (386.08 Da, theory), indicating an Oz_1Tz_2 structure. The intermediate with two rings formed has increased by both 386 (two alkylations) and 579 Da (three alkylations), showing a population of Oz_1Tz_1 and Tz_2 in roughly a 1:1 mixture. The species with one ring formed shows some minor heterogeneity, undergoing three and four alkylation events in a ratio of ~9:1. This one ring intermediate is then a 9:1 mixture resulting from cyclization of a Cys residue (at one site or multiple sites) and cyclization of a Ser residue. As an internal control, the intermediate with zero rings (i.e., starting substrate) formed has increased in mass by 772.19 Da (772.15 Da, theory), verifying that all four thiols were available and not prevented from reaction by intra- or intermolecular disulfides bonds. These data can be translated into Scheme 2 below. Additionally, processing of a $Ser^{65} \rightarrow Cys^{65}$ mutant substrate for 5 h gave the seven biosynthetic intermediates in roughly equimolar ratios (data not shown). Treatment of this mixture with (iodoacetamido)-salicylic acid indicated that the Cys^{65} is processed as fast as other Cys residues (48, 51, and 55).

MS/MS Microcharacterization of Microcin Biosynthetic Intermediates To Localize Heterocycles. For FTMS with an external ESI source, ions can be accumulated in the ion guides external to the magnetic field (*26*) or in the ion cell inside the bore of the magnet. For the His_6-McbA substrate (88 residues) after 5 h of processing with microcin synthetase, the ESI/FT mass spectrum of the microcin population acquired in the external ion accumulation mode yielded the 8+, 7+, 6+, 5+, and 4+ charge states (Figure 5a). A spectrum of a similar sample (12 h of enzymatic processing) acquired in the internal ion accumulation mode yielded the

Scheme 2: Processing Pathway Based on Data in Figure 4c[a]

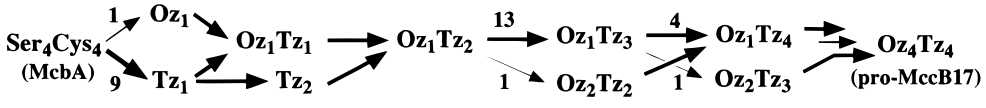

[a] Abbreviations: Oz, oxazole; Tz, thiazole. Subscripts denote number of rings, not their position in substrate 88mer.

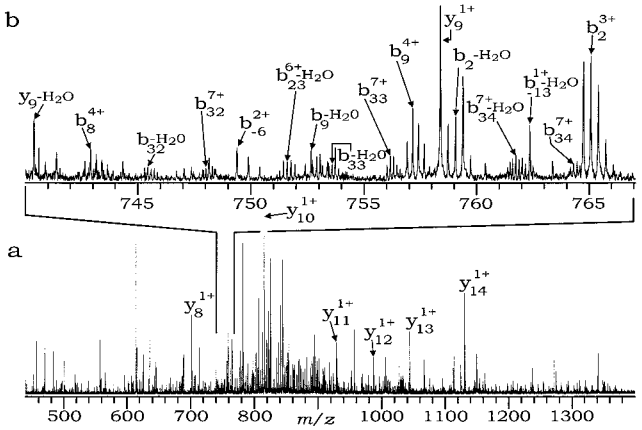

FIGURE 6: (a) Broadband spectrum from nozzle−skimmer dissociation of disulfide-intact His_6-McbA ions of Figure 1. (b) Expansion of *m*/*z* 740−767; b- and y-type ions contain the N- and the C-terminus, respectively; arrow, most abundant isotopic peak for a distribution.

10+, 9+, 8+, 7+, and 6+ charge states (Figure 5b). This charge reduction effect by the external ion accumulation process has been reported previously (*19*) and markedly reduces the abundance of the higher charge states (e.g., the 9+ ions); these higher charge states (lower *m*/*z* ratios) fragment more efficiently and in more amide bond positions during MS/MS (*27*). For MS/MS in this study, the 9+ ions of His_6-McbA from internal ion accumulation gave the best fragmentation data, with the 8+ and 7+ ions from external accumulation providing few informative fragment ions.

Fragmentation of the 9+ ions of disulfide-intact His_6-McbA without enzyme treatment by nozzle−skimmer (NS) dissociation in the ESI source region yielded the Figure 6a spectrum. Over 160 distinct isotopic distributions were measured for the 47 unique fragment ions that are mapped to the primary sequence of the 88 residue His_6-McbA in Figure 7a. Polypeptide ions dissociate primarily by cleavage of amide bonds, generating product ions containing either the N- or the C-terminus, designated b- or y-type ions, respectively (Scheme 3) (*28*). No b or y fragment ion was observed between Cys^{41} and Cys^{55}, probably due to the presence of the two disulfide bonds; reduction of these prior to ion fragmentation yielded b and y ions inside this region (Figure 7a, dotted bars; spectrum not shown). For MS/MS of biosynthetic intermediates, any b- or y-type ions resulting from amide bond cleavage between Gly^{39} and Ser^{64} (see Scheme 1) will reveal the number of rings within the cyclization sites contained in that fragment ion.

The 1−7 ring MccB17 intermediates shown in Figure 2 are not separable by HPLC. However, removal of the His_6-tag and the leader peptide using α-chymotrypsin gave MccB17 with an extra N-terminal Gly (asterisk in Figure 7a) relative to wt MccB17 and an observed M_r value of 3310.29-*0* Da (3310.26-*0* Da, theory). Cleavage of the leader allowed HPLC fractionation of the biosynthetic intermediates (not shown), but MS/MS of the 4+ ions of these intermediates resulted primarily in ejection of neutrals ($-H_2O$ and $-NH_3$). Additionally, extended chymotryptic digestion of unprocessed His_6-McbA did not cleave the Gln−Gly or Asn−Gly bonds in the cyclization region, reportedly minor activities of α-chymotrypsin (*29*). Thus, MS/MS was utilized to cleave amide bonds between the sites of ring formation.

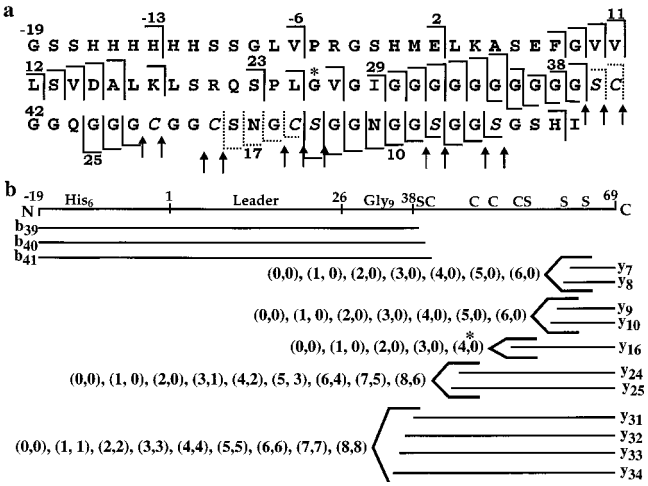

FIGURE 7: (a) Correlation of observed fragment ions from collisional (SORI) and photodissociation (IRMPD) of (processed) His_6-McbA to its primary sequence; bar facing left, b-type ion; bar facing right, y-type ion; dotted bars, fragment ion only observed if disulfides are reduced prior to ion fragmentation; arrows, amide bond sites deleted or stabilized by heterocyclization (*9*); asterisk, extra Gly residue (vs wild-type Microcin B17) left after α-chymotryptic cleavage of the leader peptide. (b) Summary of ring content determined for the most informative fragment ions; number pairs in parentheses follow this syntax: (ring content of the precursor His_6-McbA ions, ring content of the fragment ion). For example, the (6,4) designation for the y_{25} ion was obtained from fragmentation of the six ring species from Figure 2. In this MS/MS spectrum, the y_{25} ion was observed and indicated a ring content of four (Figure 8a). There are six possible ring formation sites in this C-terminal piece of the molecule (see single-letter codes for Cys or Ser at the top right of Figure 7b), but only four have actually formed.

Scheme 3: Nomenclature for Fragment Ions Produced from Low-Energy Dissociation of Peptide Ions

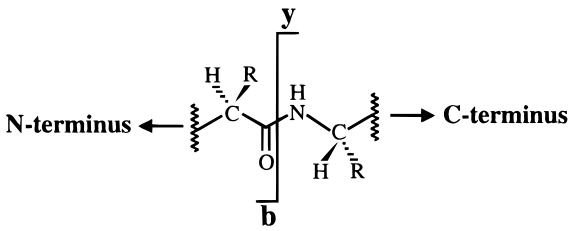

Previously, we have shown that the effect of heterocyclization on MS/MS fragmentation is to block cleavage at the amide bond deleted by ring formation and at the amide bond downstream from, and in conjugation with, the heterocycle (*9*). Thus, compared to unmodified His_6-McbA substrate which fragments at defined amide bonds (Figures 6 and 7a), the signature of a thiazole or oxazole heterocycle is the absence of two fragments. All possible amide bonds that could be so blocked from fragmenting are indicated with arrows in Figure 7a. Alternatively, a fragment ion remote from (but containing) a ring formation site can be compared to the Figure 6 control spectrum and the ring content determined by the integer of 20 Da losses.

As an initial test of MS/MS, the 9+ ions of the six ring intermediate were isolated[2] and dissociated using infrared photons (IRMPD) or collisions with argon (SORI). The IRMPD spectrum (Figure 8) shows many of the same fragment ions observed for MS/MS of the unprocessed substrate. However, the b_{39}, b_{40}, and b_{41} ions are completely prevented from forming, indicating that both rings in the

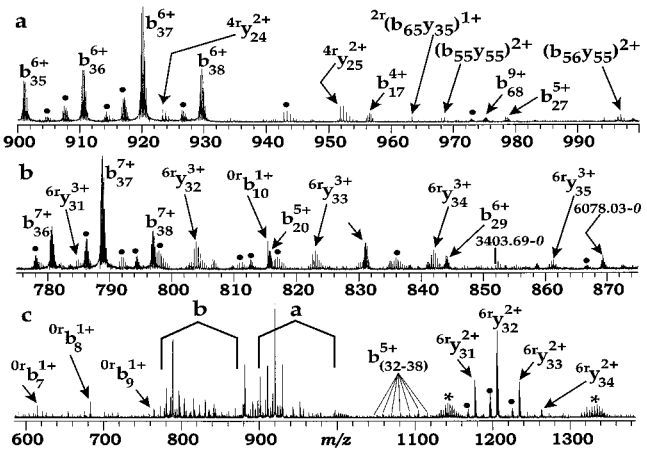

FIGURE 8: Photodissociation spectrum of the His_6-McbA intermediate with six rings formed; dots, water (−18) and ammonia (−17) losses; 9.4 T data, 67 scans. The full spectrum is displayed at the bottom, with expansion of *m*/*z* regions 900−1000 and 775−875 shown in (a) and (b), respectively.

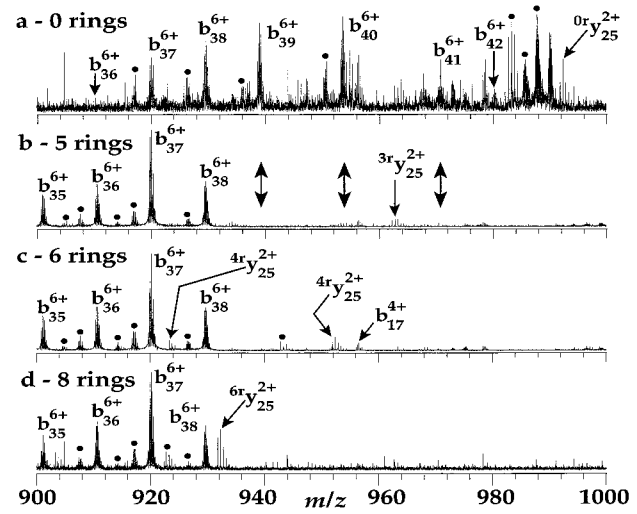

FIGURE 9: Partial photodissociation spectra of His_6-McbA with 0 (a), 5 (b), 6 (c), and 8 (d) rings formed; dots, water (−18) and ammonia (−17) losses; double-headed arrows, predicted positions of b_{39}, b_{40}, and b_{41} fragment ions; 9.4 T data with 22, 66, 67, and 34 scans, from top to bottom, respectively.

N-terminal bisheterocyclization site have formed in this intermediate. Further, two doubly charged fragment ions at *m*/*z* 924 and 952 would be consistent with the y_{24} and y_{25} ions, respectively, if they contained four heterocyclic rings (−80.08 Da vs 80.12 Da, theory). These y-type fragment ions include the six C-terminal ring formation sites (Figure 7a); therefore, in the six ring species, four rings are in the last six sites. The singly charged y_{10}, y_9, and y_8 fragment ions have the same M_r values as these ions formed from unprocessed His_6-McbA ions. For these fragment ions, there is no evidence for −20 Da satellite peaks, indicating that neither of the C-terminal Ser residues have cyclized. So for the six ring intermediate, the six most N-terminal rings have formed.

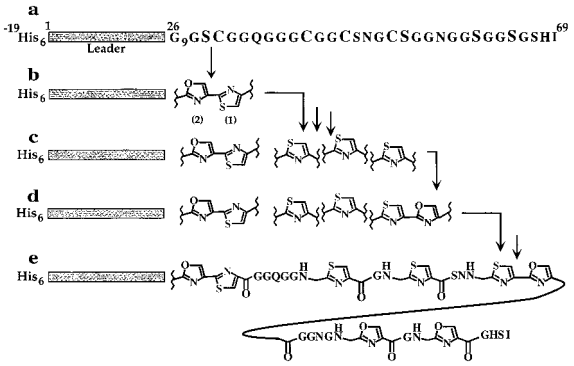

FIGURE 10: Schematic of the major processing pathway of the His_6-McbA substrate by Microcin B17 synthetase as determined by alkylation and MS/MS experiments.

Comparing fragmentation spectra of intermediates with five and six rings (Figure 9) with the MS/MS spectra from the starting material and the eight ring final product species, the y_{25} fragment ion (and its −18 water loss peak) shifts by different increments of 20 Da. For the five ring intermediate, the two N-proximal rings (the 4,2-OzTz) have formed (no b_{39}, b_{40}, b_{41} ions), and the y_{25} indicates that three rings are present in the last six sites. Again, the y_{25} ion shows that neither C-terminal oxazole (sites 7 and 8) has formed (not shown). MS/MS of the two ring intermediate gives a simple pattern: there is an absence of the b_{39}, b_{40}, and b_{41} ions (data not shown but tabulated in Figure 7b), revealing that Ser and Cys at $Gly^{39}Ser^{40}Cys^{41}$ have been processed to the tandem bisheterocycle. Additionally, MS/MS of the alkylated species with one and two alkylation events did not yield any further information. In aggregate, this information is summarized in Figure 7b in which subsets of observed b ions and y ions ($y_{7,8}$; $y_{9,10}$; y_{16}; $y_{24,25}$; y_{31-34}) that are diagnostic for heterocycle localization are grouped underneath the ring formation sites they contain. These data define the directionality of microcin heterocyclization shown in Figure 10.

DISCUSSION

Distributivity. This work analyzes the progressive introduction of 8 heterocycles into McbA by the pure 3 subunit microcin synthetase, ultimately modifying 14 of 43 residues of the mature antibiotic (Microcin B17). Mass spectrometric analysis of these posttranslational ring formations shows clear evidence that all intermediates (one to seven rings) accumulate in solution. Since each intermediate is present in the same order-of-magnitude concentration (e.g., the 16.5 h data of Figure 2) and the enzyme-to-substrate ratio is <1:1000, then the Figure 2 data indicate that for each binding/catalytic event between the synthetase complex and its substrate, only one ring is made before nascent product is released. Over time, early intermediates disappear, and intermediates with more rings appear and are swept through to the final eight ring product, consistent with the released intermediates being on the pathway to antibiotic. Therefore, MccB17 synthetase is distributive in each of its eight ring-forming steps; that is, the k_{off} for each of the 1−7 ring intermediates is faster than each k_{cat} for the ring-forming

[2] Some ions from other charge states that should have been removed during the isolation procedure are visible in the IRMPD spectrum (Figure 8, labeled with asterisks). A control spectrum (67 scans) with no laser shots showed the isolation procedure to have completely removed all ions except those targeted for dissociation (not shown). Further, the SORI spectrum showed no evidence of these contaminating charge states and corroborated the IRMPD results, albeit with lower fragment ion signal-to-noise ratios. The contaminating ions could result from infrared photons dissociating noncovalent clusters of analyte ions that were not ejected during the isolation procedure due to their high *m*/*z* values (i.e., >2000 *m*/*z*).

steps. There may be a small bias in favor of ring-containing molecules for subsequent rounds of cyclization. For example, the 16.5 h time point of Figure 2 shows a nearly equal abundance of all intermediates; a simple model using a single rate constant for all cyclizations predicts far greater depletion of early intermediates before later intermediates are detectable. Without physical isolation and detailed analysis of their catalytic efficiency for further conversion, one cannot a priori distinguish between k_{cat} and K_M effects for any preferential recognition. However, the two chemical reactions occurring (Tz vs Oz ring formations) are related but distinct, the first steps of which involve nucleophilic attack by Cys (thiolate for thiazole) or by Ser (alkoxide for oxazole). The observed pattern of biosynthetic intermediates in part reflect the chemoselective processing of Cys residues faster than Ser residues. Note also that the six ring intermediate apparently builds up to ~3-fold higher abundance than other intermediates in both the 16.5 h and the 20.5 h time points (Figure 2 and the data of Figures 3b and 4) and that is then presented for Ser^{62} and Ser^{65} cyclization.

While the initial MS analysis serves to count the number of rings in the intermediates by increments of 20 mass units/ring formed (from M to M−160 Da), sorting into oxazole or thiazole was done by MS analysis after subsequent alkylation of the remaining cysteine thiols. These two sets of data allowed the following conclusions. In the first ring-forming step, there is a ~9/1 preference for thiazole over oxazole. At the two ring intermediate, one Ser and one Cys have been cyclized. Then rings 3, 4, and 5 are thiazole formations. The last three rings, 6, 7, and 8, are oxazoles. The chemoselectivity bias (Cys > Ser) is as one would expect from both pK_a considerations (Cys-SH p$K_a \approx 7$, Ser-OH p$K_a \approx 13$) and higher nucleophilicity of thiolate over alkoxide. One serine is anomalously reactive for heterocyclization and that may be driven by a different constraint, one of directionality (as discussed below).

From the dynamic range of the 9.4 T instrument, we could detect as little as a 1% component in a complex mixture (Figure 4c). These low-level species indicate that the synthetase does not exercise strict control over the processing. There are parallel/convergent pathways operative for intermediate formation and conversion in the maturation of MccB17.

To establish the timing of individual ring formation in microcin intermediates, we utilized high-resolution tandem MS coupled with the knowledge that one ring formation results in the absence of fragment ions from two peptide bond cleavages (*9*). For these MS/MS experiments, the His_6-tag was probably advantageous, as its presence adds protonation sites, giving more highly charged analyte ions which fragment more efficiently and in more amide bond locations (*27*). The first two rings formed are at Ser^{40} and Cys^{41}, the most amino proximal of the cyclizable side chains and the ones closest to the high-affinity N-terminal propeptide (residues 1−26) in substrate McbA. The next intermediate structure that was clearly elucidated was the five ring species in which the next three downstream cysteines, Cys^{48}, Cys^{51}, and Cys^{55}, have all been converted to thiazoles. At this point, all the cysteines have been cyclized, but only one of the serines (Ser^{40}). The six ring intermediate continues the overall N→C directionality because Ser^{56} is cyclized next, producing the second pair of 4,2-fused bisheterocycles. The most carboxy-proximal sites, Ser^{62} and Ser^{65}, are clearly cyclized last. Although in principle the MS/MS fragmentation approach could also provide sequence information on the timing of the other ring formations (e.g., 3→4 ring; 4→5 ring), at present we do not see enough amide bond cleavages to know if Ser^{40} is cyclized before Cys^{41} and whether there is precise N→C directionality among the three cysteines at positions 48, 51, and 55, or whether Ser^{62} is preferentially cyclized before Ser^{65}.

There appears to be a general effect of ring formation that suppresses fragment ion formation such that the higher the heterocyclic content, the lower the fragment ion yields. Specifically, the intensity of the y_{7-10} ions became smaller as the ring content increased from five to eight rings. Additionally, the y_{20}, y_{17}, and y_{16} ions were detected only for intermediates with two rings or less, with one exception; the y_{16} ion was observed with a 5:1 signal-to-noise ratio for the intermediate with four rings (asterisk, Figure 7b). This is evidence for a preferred N→C processing of cysteines 48, 51, and 55. Reliable detection of the y_{20}, y_{17}, and y_{16} ions from the three, four, and five ring species would have determined the degree of directionality for thiazole formation within this "Cys box" region. Perhaps MS/MS using ESI/FTMS at higher magnetic field or further MS/MS attempts (at 9.4 T) of the Figure 3 alkylated species (Oz_1Tz_1, Oz_1Tx_2, and Oz_1Tz_3) could detect the critical fragment ions for elucidation of the Cys box processing order.

Overall Processing Model. Coupling the alkylation and the MS/MS data, the pattern of processing depicted in Figure 10 was formulated, with a preferred cyclization order (numbering ring formation sites from N→C) of 2, 1, (3, 4, 5) 6, (7, 8). The amino-proximal bisheterocyclic site is made first with a preferred C→N kinetic pathway (Tz > Oz), similar to that observed for the $McbA_{1-46}$-truncated substrate (*9*). Then the third, fourth, and fifth rings formed are primarily thiazoles. Somewhat surprisingly, the oxazole at site 6 (Ser^{56}) is made before either of the isolated Ser residues (Ser^{62}, Ser^{65}) can cyclize. Formation of site 6 involves cyclization onto a conjugated amide by the alkoxide, found to occur slowly, or not at all, in different sequence contexts (*9*). Since k_{cat} is probably decreased considerably for this step, an enhanced K_D for this site must exist. The two mono-oxazoles are formed last, and apparently, formation of the seventh ring is the slowest step in the processing, as the six ring species accumulates (Figure 2, middle). The slow conversion of Ser^{62} and Ser^{65} to the seven ring and eight ring forms of MccB17 parallels overproduction results in vivo where six, seven, and eight ring microcins were detected and likewise found to form the C-terminal oxazole last. Since the six, seven, and eight ring forms of MccB17 have antibiotic activity (*25*), there may be no premium for *E. coli* to increase the catalytic efficiency to form the last two oxazoles. When Ser^{65} is mutated to Cys, the latter cyclizes faster so chemoselectivity takes precedence over directionality. The preferential cyclization of Ser^{40} before Ser^{56} may reflect some functional driving force for 4,2-tandem bisheterocycle formation.

A distributive mechanism for MccB17 biosynthesis could result in toxicity of partially cyclized microcins as they build up in the producing cell. It appears that the 4,2-thiazole−oxazole from $Gly^{54}Cys^{55}Ser^{56}$ is required for antibiotic activity (*25*), so intermediates earlier then this six ring form

of MccB17 may not be toxic. Six, seven, and eight ring forms are exported by the McbE and -F export system and presumably do not accumulate in the producer cell. Finally, one could conjecture that an eight Cys McbA would be more efficiently cyclized to an eight ring MccB17 species but the tandem oxazole−thiazole and thiazole−oxazole pairs may not be replaceable with bithiazole without reducing antibiotic activity.

ACKNOWLEDGMENT

FTMS access and support were facilitated by Mark Emmett, John Quinn, and Alan Marshall (9.4 T); Roman Zubarev, Einar Fridriksson, and Fred McLafferty (6.1 T; Cornell University); and Gary Kruppa, J. Paul Speir, Sunia Afzall, and Frank Laukien (4.7 T; Bruker Daltonics). We thank Jill Milne for the His_6-McbA plasmid, Ranabir Sinha Roy for the pCalBCDn plasmid, and Deborah Zamble, Ranabir Sinha Roy, and Florian Hoffelder for critical reading of this manuscript.

REFERENCES

1. Moreno, F., San Millan, J. L., Hernandez-Chico, C., and Kolter, R. (1995) in *Genetics and Biochemistry of Antibiotic Production* (Vining, L. C., and Stuttard, C., Eds.) pp 307−321, Butterworth-Heinemann, Boston.
2. Vizan, J. L., Hernandez-Chico, C., del Castillo, I., and Moreno, F. (1991) *EMBO J. 10*, 467−476.
3. Yorgey, P., Davagnino, J., and Kolter, R. (1993) *Mol. Microbiol. 9*, 897−905.
4. Yorgey, P., Lee, J., Kordel, J., Vivas, E., Warner, P., Jebaratnam, D., and Kolter, R. (1994) *Proc. Natl. Acad. Sci. U.S.A. 91*, 4519−4523.
5. Milne, J. C., Eliot, A. E., Kelleher, N. L., and Walsh, C. T. (1998) *Biochemistry 37*, 13250−13261.
6. Madison, L. L., Vivas, E. I., Li, Y. M., Walsh, C. T., and Kolter, R. (1997) *Mol. Microbiol. 23*, 161−168.
7. Sinha Roy, R., Kim, S., Baleja, J. D., and Walsh, C. T. (1998) *Chem. Biol. 5*, 217−228.
8. Belshaw, P. J., Sinha Roy, R., Kelleher, N. L., and Walsh, C. T. (1998) *Chem. Biol. 5*, 373−384.
9. Kelleher, N. L., Belshaw, P. J., and Walsh, C. T. (1998) *J. Am. Chem. Soc. 120*, 9716−9717.
10. Marshall, A. G., and Grosshans, P. B. (1991) *Anal. Chem. 63*, 215A−229A.
11. Fenn, J. B., Mann, M., Meng, C. K., and Wong, S. F. (1990) *Mass Spectrom. Rev. 9*, 37−70.
12. McLafferty, F. W. (1994) *Acc. Chem. Res. 27*, 379−386.
13. Li, Y. M., Milne, J. C., Madison, L. L., Kolter, R., and Walsh, C. T. (1996) *Science 274*, 1188−1193.
14. Sinha Roy, R., Belshaw, P. J., and Walsh, C. T. (1998) *Biochemistry 37*, 4125−4136.
15. Higuchi, R. (1989) *Using PCR to Engineer DNA*, Stockton Press, New York.
16. Wilm, M., and Mann, M. (1996) *Anal. Chem. 68*, 1−8.
17. Kofel, P., Allemann, M., Kellerhals, H. P., and Wanczek, K. P. (1989) *Int. J. Mass Spectrom. Ion Processes 87*, 237−247.
18. Beu, S. C., Senko, M. W., Quinn, J. P., and McLafferty, F. W. (1993) *J. Am. Soc. Mass Spectrom. 4*, 190−192.
19. Senko, M. W., Hendrickson, C. L., Pasa-Tolic, L., Marto, J. A., White, F. M., Guan, S., and Marshall, A. G. (1996) *Rapid Commun. Mass Spectrom. 10*, 1824−1828.
20. Loo, J. A., Udseth, H. R., and Smith, R. D. (1988) *Rapid Commun. Mass Spectrom. 2*, 207−210.
21. Senko, M. W., Beu, S. C., and McLafferty, F. W. (1995) *J. Am. Soc. Mass Spectrom. 6*, 229−233.
22. Marshall, A. G., Wang, T.-C. L., and Ricca, T. L. (1985) *J. Am. Chem. Soc. 107*, 7893−7897.
23. Gauthier, J. W., Trautman, T. R., and Jacobson, D. B. (1991) *Anal. Chim. Acta 246*, 211−225.
24. Little, D. P., Speir, J. P., Senko, M. W., O'Connor, P. B., and McLafferty, F. W. (1994) *Anal. Chem. 66*, 2809−2815.
25. Sinha Roy, R., Kelleher, N. L., Milne, J. C., and Walsh, C. T. (1999) *Chem. Biol. 6*, 305−318.
26. Senko, M. W., Hendrickson, C. L., Emmett, M. R., Shi, S. D.-H., and Marshall, A. G. (1997) *J. Am. Soc. Mass Spectrom. 8*, 970−976.
27. Senko, M. W., Speir, J. P., and McLafferty, F. W. (1994) *Anal. Chem. 66*, 2801−2808.
28. Roepstorff, P., and Fohlman, J. (1984) *Biomed. Mass Spectrom. 11*, 601.
29. Keil, B. (1992) *Specificity of Proteolysis*, Springer-Verlag, New York.

BI9913698